Draft version January 25, 2006
Preprint typeset using LaTeX style emulateapj v. 6/22/04

STOPPING COOLING FLOWS WITH JETS

Fabrizio Brighenti[1,2], William G. Mathews[1]

Draft version January 25, 2006

ABSTRACT

We describe 2D gasdynamical models of jets that carry mass as well as energy to the hot gas in galaxy clusters. These flows have many attractive attributes for solving the galaxy cluster cooling flow problem: Why the hot gas temperature and density profiles resemble cooling flows but show no spectral evidence of cooling to low temperatures. Using an approximate model for the cluster A1795, we show that mass-carrying jets can reduce the overall cooling rate to or below the low values implied by X-ray spectra. Biconical subrelativistic jets, described by several *ad hoc* parameters, are assumed to be activated when gas flows toward or cools near a central supermassive black hole. As the jets proceed out from the center they entrain more and more ambient gas. The jets lose internal pressure by expansion and are compressed by the ambient cluster gas, becoming rather difficult to observe. For a wide variety of initial jet parameters and several feedback scenarios the global cooling can be suppressed for many Gyrs while maintaining cluster temperature profiles similar to those observed. The intermittancy of the feedback generates multiple generations of X-ray cavities similar to those observed in the Perseus Cluster and elsewhere.

Subject headings: X-rays: galaxies – galaxies: clusters: general – X-rays: galaxies: clusters – galaxies: cooling flows

1. INTRODUCTION

Many computationally elaborate calculations of jet-heated cooling flows have been proposed to explain why the hot gas in galaxy clusters cools much slower than the rate expected from the cluster X-ray luminosity, $\dot{M}_{cf} \approx (2\mu m_p/5kT_{vir})L_x$ (e.g. Cavaliere et al. 2001; Reynolds, Heinz, & Begelman 2001,2002; Bruggen & Kaiser 2002; McCarthy et al. 2003; Hoeft et al. 2003; Basson & Alexander 2003; Omma et al. 2004; dalla Vecchia et al. 2004; Zanni et al. 2005). In principle the energy created by gas accreting at rates very much less than $\dot{M}_{cf}$ onto supermassive black holes in cluster-centered galaxies can easily balance the radiative losses L_x. Consequently, AGN jets have been regarded as a plausible means to distribute this energy throughout the cluster gas. Unfortunately, few if any jet-heated flow simulations closely resemble in projection the X-ray emission and radial temperature profiles observed in galaxy groups and clusters. Surprisingly often these calculations do not include radiative losses and therefore lack the essential physics to prove that cooling can be stopped by the jets. Nor do these calculations typically continue for many Gyrs. Multi-Gyr calculations are essential to determine if the proposed type of heating can keep the group/cluster gas from cooling while also preserving time-averaged temperature and entropy profiles commonly observed, most of which are very similar. In general, the long term effectiveness of powerful jet heating in stopping the cooling has not been convincingly demonstrated. As a first step toward a more successful solution, adopted here, jet-heating scenarios are sought that are consistent with the global observations of the hot cluster gas. Once this problem is solved, the next step is to determine if real black holes can indeed supply energy in the form and amount required.

We consider here jet-dominated flows in which gas near the cores of cluster-centered elliptical galaxies is accelerated in bipolar outflows when triggered by a supermassive black hole feedback mechanism. Both mass and energy are transported out from the center. The feedback appears largely as an outward flow of mass rather than energy, although the energetics of successful flows must be understood *a postiori*. We find that these more massive jets have many desirable long term attributes. We have discussed elsewhere how heated, buoyant gas can rise upstream in cooling flows, transporting mass and energy to distant cluster gas in a manner that sharply reduces the overall cooling rate and preserves the thermal profiles observed (Mathews, et al. 2003; Mathews, Brighenti & Boute 2004). We now turn our attention to the possibility that mass-loaded subrelativistic jets can accomplish the same desirable results.

Another inspiration for the calculations described here are recent HI (Morganti et al. 2004; 2005), UV (e.g. Crenshaw et al. 1999; Kriss 2003) and X-ray (George et al. 1998; Risaliti et al. 2005) observa-

[1] University of California Observatories/Lick Observatory, Department of Astronomy and Astrophysics, University of California, Santa Cruz, CA 95064
[2] Dipartimento di Astronomia, Università di Bologna, via Ranzani 1, Bologna 40127, Italy

tions of AGNs showing blue-shifted absorption or emission lines along the line of sight. Neither the optical depth nor the covering factor of the outflowing gas can be accurately determined from these observations, but the outflowing mass flux can be comparable to the Eddington limit, implying that relatively little gas is being directly accreted by the central black hole. The outflow velocity is typically several 100 km s^{-1} but increases to several 1000 km s^{-1} in a few more luminous objects (Kriss 2004). At least half of all AGNs exhibit outflows so it is plausible that they exist in all objects and with substantial covering factors. Winds from accretion disks are one possible explanation for the outflows (Narayan & Yi 1994; Konigl & Kartje 1994; Blandford & Begelman 1999; Proga 2000; Soker & Pizzolato 2005), particularly those with higher velocities.

The highly uncertain outflowing mass flux observed in low luminosity galaxies ($\dot{M} \sim 1\ M_\odot\ \mathrm{yr}^{-1}$), is far less than the mass flux that arrives at the central galaxies in group and cluster cooling flows, $\dot{M} \sim 10 - 300\ M_\odot\ \mathrm{yr}^{-1}$. However, outflowing gas in these more massive flows is likely to be too hot, too rarefied and too highly ionized to produce blueshifted UV or X-ray lines and would be difficult to observe. Indeed, currently available UV and X-ray absorption observations may naturally select the densest, coldest and most slowly moving gas in each outflow. Many authors (e.g. Churazov et al. 2002; 2005; Peterson & Fabian 2005) argue that the mechanical outflow luminosity L_{mech} from massive black holes can greatly exceed their bolometric luminosity, and this may apply to all radiatively inefficient black holes (Hopkins et al. 2005).

As in the Blandford-Begelman accretion model, we assume that the majority of gas accreted at the outer edges of the accretion disks ultimately flows away from the disk surface as a fast but nonrelativistic wind. Such disk flows are unlike the relativistic $e^{\pm}$ radio-emitting jets driven from much smaller regions near the central hole (Blandford & Znajek 1977), but the two types of outflow may coexist. In contrast, winds driven by radiation pressure from thin disks, such as those described by Proga (2000) are confined by strong radial, polodial fields (e.g. Blandford & Payne 1982), and may be directed mostly along the equatorial plane. However, more axis-oriented outflows may be possible from thicker disks or with different, more vertical field geometries (e.g. Everett, Königl & Kartje 2001). Nevertheless, fast wind-driven bipolar flows, such as we consider, may at their origin fill cones of significant solid angles. For example, Proga (2003) finds that most of the mass flux in disk winds at high velocities $v \gtrsim 1000$ km/s, which we require in our flows, lies within 20 or 30 degrees from the polar axes. Such broad outflows are expected to entrain additional ambient gas as they proceed out from the central region. Therefore, for our exploratory calculations we adopt a bipolar wind geometry similar to the prevailing geometry in models of jet-heated cooling flows cited above, but allow the jets to have larger angular sizes at their source. Most of the mass outflow in our jets arises not from the origin but by entrainment of ambient gas at larger radii – such a model is supported by the recent observations of Sun, Jerius & Jones (2005) discussed below. Omma et al. (2004) considered the initial transient flow resulting from a bipolar outflow of this sort, but did not address the important question whether or not such jets can shut down the cooling flow for many Gyrs while preserving the observed thermal gradient in the hot gas. This is our objective here.

In the 2D gasdynamical models described here nonrelativistic outflows are generated by assigning a fixed velocity to gas that flows into a biconical source region (radius of a few kpc with half angle $\theta_j \sim 5 - 20^\circ$) at the cluster center. The acceleration of gas in the source bicone is activated by a feedback recipe triggered as gas flows into the innermost zones. The 2D biconical outflows, which may for example represent a disk wind, proceed along the axis of symmetry of the computational grid. Even when the initial outflow has rather substantial opening angles (i.e. $\theta_j \sim 20^\circ$), the flow rapidly concentrates within ~ 30 kpc into a much narrower jet. This compression occurs because the rapid pressure drop in the jet due to expansion causes the jet to be compressed and narrowed by the ambient gas pressure which decreases less rapidly with radius in the cluster gas. As the jet proceeds, it entrains additional ambient gas and its mass flux increases. These solutions have two excellent attributes: after many Gyrs the time-averaged gas temperature profile resembles those observed, $dT/dr > 0$ in $r \lesssim 0.1 r_{vir}$, and very little gas cools below $\sim T_{vir}$. The jet itself is difficult to observe. Finally, because of the intermittent nature of the feedback jet excitation, multiple generations of large X-ray cavities are created with 2 or 4 visible at any time, very similar to Perseus (e.g. Fabian et al. 2005).

2. THE CLUSTER A1795

We compare our gasdynamical calculations with the temperature and density profiles of the well-observed cluster Abell 1795 (Tamura et al. 201; Ettori et al. 2002) assumed to be at a distance 243 Mpc. Abell 1795 is a typical rich cluster with a central cD galaxy and a reasonably relaxed overall structure (Boute & Tsai 1996). Abell 1795 has the usual attributes of normal cooling flows: strong central peak in X-ray surface brightness (e.g. Tamura et al. 2001), a positive temperature gradient dT/dr in the central regions out to ~ 500 kpc, a central radiative cooling time $\sim 3 \times 10^8$ yrs that is much less than the cluster age (e.g. Edge et al. 1992; Fabian et al. 2001), optical line emission near the central cD (Cowie et al. 1983), an excess of blue and ultraviolet light possibly from massive young stars (Johnstone, Fabian & Nulsen 1987; Cardiel, Gor-

gas & Aragon-Salamanca 1998; Mittaz et a. 2001) and a central radio source 4C 26.42 (McNamara et al. 1996a,b). Chandra images near the center of Abell 1795 reveal an X-ray emission feature aligned with a remarkable optical filament (Fabian et al. 2001). This filament and the central total mass profile, $M \propto r^{0.6}$ inside 40 kpc, which is somewhat flatter than NFW (Navarro, Frenk & White 1996), may suggest a local deviation from hydrostatic equilibrium.

We approximate the total mass profile in A1795 with an NFW profile with virial mass $M_{vir} = 10^{15}\ M_\odot$ and concentration $c = 6.57$, which also matches the total mass found from X-ray observations, assuming hydrostatic equilibrium. The de Vaucouleurs mass profile of the central cD galaxy, defined by $M_* \sim 6 \times 10^{11}$ and $R_e = 8.5$ kpc, has also been included, but this mass has little effect on the overall gas dynamics.

3. COMPUTATIONAL PROCEDURE

The two-dimensional numerical calculations described here are solutions of the same flow equations described in our earlier paper on heated cooling flows (Brighenti & Mathews 2002). These equations explicitly include radiative cooling. The 2D computational grid is in spherical polar coordinates r and θ. Unless stated otherwise, the grid is comprised of 200 logarithmically spaced radial zones extending to 3 Mpc and having a central zone of size 0.75 kpc. There are 60 evenly spaced angular zones in the range $0 < \theta < \pi$. Some of our flows have been computed at higher resolution with 600 logarithmically spaced radial zones extending to 3 Mpc, with a central zone of size 0.6 kpc, and 120 evenly-spaced angular zones. We find that all important results (temperature and density profiles, cooling rate, etc.) are essentially unchanged when the resolution is improved.

When gas in a computational zone begins to cool by radiative losses to low temperatures, usually near the center of the flow, the density of cooling gas in the zone increases to maintain pressure equilibrium with gas in neighboring grid zones. This representation of the cooling process, discretized and averaged on the grid scale, is unphysical since gas cooling in pressure equilibrium should eventually occupy a volume much smaller than that of the grid zones. In order to approximately allow for this subgrid evolution, we remove cold gas as it forms, assuming that its volume becomes vanishingly small. Cooling gas is removed by adding a mass sink term to the equation of continuity, $-q(T)\rho/t_{cool}$, where t_{cool} is the local radiative cooling time as described by Brighenti & Mathews (2002) and $q = 2\exp(-T/T_q)^2$ becomes large when $T \lesssim T_q = 5 \times 10^5$ K. This mass sink term is used to remove the unphysical clutter of zones containing cold gas without affecting the flow of hotter gas, $T \gg T_q$, throughout the rest of the cluster.

In some calculations unphysical cooling also occurs (generally at small radii) along the symmetry axis, $\theta = 0$ or π, where we employ reflection boundary conditions. As gas approaches a reflecting axis, it is compressed and cools in a way that would not occur in a full 3D calculation where such reflections do not occur. Nevertheless, this spurious, purely numerical cooling near the symmetry axis is necessarily included in the computations described below. Consequently, our estimates of the cooling rate $\dot{M}$ may be regarded as conservative upper limits. When the flow velocity is entirely radial, as in the (unheated) cooling flow described in the next section, this type of boundary cooling does not occur.

4. NORMAL COOLING FLOW IN A1795

We begin with a simple evolutionary cooling flow for A1795 in which the gas is allowed to evolve from an initial hydrostatic model in good agreement with the observed density and temperature profiles. In this traditional spherical cooling flow all the gas cools at the center of the flow and there is no dependence on polar angle θ. For standard cosmological parameters ($\Omega = 0.3$; $\Lambda = 0.7$; $H = 70$ km s^{-1} Mpc^{-1}) large clusters like Abell 1795 formed relatively recently, so we consider the internal flow evolution for only 7 Gyrs. The dotted lines in Figure 1 show the radial variation of the gas density and emission-weighted temperature in the cooling flow after 7 Gyrs. The gas density follows the observations fairly well beyond about 50 kpc but is systematically too large closer to the center. This density excess is typical for pure cooling flows, as discussed by Mathews & Brighenti (2003). The depression of the observed (azimuthally averaged) density relative to this flow within 50 kpc may be due in part to unresolved X-ray cavities.

The cooling rate $\dot{M}(t)$ for this cooling flow, shown as a dotted line in Figure 2, increases with time, approaching $\sim 400\ M_\odot$ yr^{-1} after 7 Gyrs. This cooling rate is comparable to the cooling rate for A1795 estimated by Allen et al. (2000) from deprojected ROSAT images, $\dot{M} \sim 500\ M_\odot$ yr^{-1}. However, XMM RGS spectra show no evidence of gas with temperatures less than ~ 2 keV (Tamura et al. 2001), indicating a much smaller cooling rate, $\dot{M} < 150\ M_\odot$ yr^{-1}. This upper limit is consistent with $\dot{M} \lesssim 100\ M_\odot$ yr^{-1} estimated from Chandra observations (Ettori et al. 2002).

5. JET OUTFLOWS

Gas flows including the effects of jet momentum are solved in several stages. Each calculation begins with a static cluster atmosphere based on the observed temperature and density profiles in A1795. During time $0 < t < 1$ Gyr the configuration is allowed to evolve (without jets) toward a pure cooling flow, and later during $1 < t < 7$ Gyrs the jet momentum is activated according to a feedback criterion.

We adopt a simple computational procedure to trigger jet outflow in which all gas in a biconical jet source region near the center of the flow is set into outward motion at velocity u_j as long as some feedback criterion is satisfied. The geometrical parameters that define the jet source region are the radius r_j and the half opening angle θ_j of the jet. We consider three feedback criteria to activate the jet:

> A: The gas velocity in the jet source region is set to u_j only when the gas cooling rate $\dot{M}$ is non-zero inside a radius of 1 kpc.
>
> B: The gas velocity in the jet source region is set to u_j only when the net mass flow across a sphere of radius 1 kpc is negative (mass inflow).
>
> C: Continuous jet flow u_j in the jet source region at all times.

During times when the jet outflow is not active, gas flows through the source region in accordance with the usual gasdynamical equations. Each flow calculation is uniquely designated by $mN(X, r_j, \theta_j, u_j)$ where N is a number assigned to each computed flow, $X = A$, B or C is the feedback criterion, r_j is the jet radius in kpc at the source, θ_j is the source jet half-angle in degrees and u_j is the jet source velocity in units of 10^3 km s^{-1}. Flows at the higher spatial resolution are designated with upper case $MN(X, r_j, \theta_j, u_j)$.

5.1. *A Representative Flow with Jet Momentum*

Among the many models with satisfactory or excellent results, we select $m1(A, 5, 10, 10)$ as representative and discuss it in more detail. The azimuthally averaged gas density and emission-weighted temperature profiles for the $m1(A, 5, 10, 10)$ flow are shown at three times in Figure 1. The global cooling rate $\dot{M}(t)$ for this flow, plotted in Figure 2, is small, indeed its time-averaged value $\langle \dot{M}(t) \rangle \approx 20\ M_\odot\ \mathrm{yr}^{-1}$ is well below the constraints imposed by XMM and *Chandra* observations. Even more remarkable, both the density and temperature profiles shown in Figure 1 retain their cooling flow appearance at time 7 Gyrs. Within about 50 kpc $n(r)$ and $T(r)$ for the $m(A, 5, 10, 10)$ flow lie between the pure cooling flow and the observations.

Figure 3 shows in more detail the 2D density structure at several times for the high resolution version of this flow, $M1(A, 5, 10, 10)$. The four panels in Figure 3 show illustrate the growth of successive generations of buoyant X-ray cavities. Cavities are associated with jet intermittancy. The evolution of the buoyant cavities away from the (horizontal) jet axis may be an artifact of the 2D reflection boundary conditions along this axis, but it is comparable to a similar deviation found in the 3D models of Bruggen et al. (2002). Nevertheless, the creation of multiple pairs of bubble cavities, similar to those in Perseus (Fabian et al. 2003), is an encouraging feature of these jet flows. Finally, we stress that these jets carry mass as well as energy to large distances from the central AGN and in this respect they differ from many previous calculations in which the jets carried little or no mass.

5.2. *Additional Jet Momentum Flows*

Table 1 summarizes some of the jet-heated flows we have calculated. For consistency, all results in Table 1 refer to flows computed at lower resolution, but are not significantly changed when the grid resolution is refined. In addition to listing the parameters that define each flow, Table 1 gives several additional global results after 6 Gyrs of jet feedback: the total energy E_{kin} supplied by the jet source, the time-averaged mechanical luminosity generated in the jet source region L_{mech}, the total mass that cooled M_{cool} after $t = 7$ Gyrs and the average cooling rate $\langle \dot{M} \rangle$, and the X-ray luminosity L_x at this same time. For many jet parameter combinations, the mean cooling rate $\langle \dot{M} \rangle$ is less than or comparable to the *Chandra* value $\dot{M} \approx 100\ M_\odot\ \mathrm{yr}^{-1}$. The mechanical energy for successful flows ranges from $\sim 0.02 L_x$ to $\sim L_x$. We stress that the condition $L_{mech} \gtrsim L_x$ that is usually required to keep jet-heated flows from cooling does not necessarily apply to our flows in which mass as well as energy is transported outward. Consequently, successful jet-advecting flows are possible even when $L_{mech} \ll L_x$. Jet mass transfer appears to be an efficient and robust way to recirculate gas and energy outward with little radiative cooling while retaining the cooling flow appearance as observed in the density and temperature profiles.

Regarding this latter important point, Figure 4 shows the gas density and temperature at time $t = 7$ Gyrs for a sample of successful and unsuccessful flows listed in Table 1. The cooling rates for these flows (sampled each 0.5 Gyr) are shown in Figure 5. In both Figures 1 and 4, the computed gas density within about 20-30 kpc from the center exceeds that observed in A1795, but this region of A1795 contains a cool, transient optical filament about 60 kpc in diameter and may be experiencing a local deviation from hydrostatic equilibrium. For many of the unsuccessful models with $\langle \dot{M} \rangle \gtrsim 100\ M_\odot$ yr^{-1}, most of the cooling occurs during one or two episodes. These flows would be regarded as successful in matching the X-ray data if they were computed for only $\sim 2-3$ Gyrs when $\dot{M}(t)$ is acceptably small, but star formation, which is likely to occur during times of enhanced cooling, would be inconsistent with optical colors of cluster-centered galaxies (e.g. McNamara 1997). Enhanced blue light from young stars typically persists for 2 - 3 Gyrs after a

starburst.

The mass M_{cool} in column (9) of Table 1 represents all the cooled gas that has been removed from the grid by the term $-q(T)\rho/t_{cool}$ in the equation of continuity. Almost all of this gas cools in the central regions. However, M_{cool} is not small and is often much larger than the mass of central black holes (or stars) in cluster-centered galaxies. However, there are reasons to believe that we have overestimated the global cooling rate in our models. For example the sink term $-q(T)\rho/t_{cool}$ in the continuity equation not only removes the cooled gas, but may also encourage local pressure gradients that stimulate additional cooling. If gas in a particular grid zone begins to cool while gas is being removed by the sink term, hot gas from adjacent zones, that would not otherwise cool, may be stimulated to flow toward the cooling zone, possibly raising the local cooling rate unrealistically. As discussed above, we also expect the computed cooling rate to be spuriously enhanced by cooling near the symmetry axis where reflecting boundary conditions must be employed. Evidence for computational overcooling is provided in the final two models listed in Table 1, m13(B,5,10,10) and m14(B,5,10,5), in which the sink term is set to zero, $q(T) = 0$. In flows with $q = 0$, M_{cool} in Table 1 represents the mass of cooled gas ($T << T_q = 5 \times 10^5$ K) that remains in the grid and goes into approximate free fall if it is not at the center. Values of M_{cool} for these flows are very small, suggesting that nonzero $q(T)$ does indeed artificially increase the cooling rate. But real cooling at some level can and does occur. Significant centrally-located cold gas and star formation are observed in many massive clusters (e.g. Edge 2001). Recent CO observations of A1795 by Salome & Combes (2004) have detected $\sim 10^{11}$ $M_\odot$ of cold gas which is entirely consistent with our flow calculations based on an approximate model for A1795.

In marked contrast to our earlier models in which we explored a wide variety of heated cooling flows (Brighenti & Mathews 2002; 2003), very few of the jet momentum flows described here have temperature and density profiles that strongly deviate from the observations of A1795. The relative success of each jet momentum flow, expressed in column (11) of Table 1, is based largely on the magnitude of the mean cooling rate $\langle \dot{M} \rangle$. The results in Table 1 and Figures 2 and 5 imply limits on the jet source parameters X, r_j, θ_j, and u_j corresponding to $\langle \dot{M} \rangle \lesssim 100$ $M_\odot$ yr^{-1} as observed with *Chandra*. In particular, radiative cooling is effectively shut down for source regions with radii $r_j \gtrsim 3$ kpc, half angles $\theta_j \gtrsim 10^o$ and jet velocities $u_j \gtrsim 5000$ km s^{-1}.

5.3. *Nature of the Jet Flow*

The simple jets we employ are based on the plausible notion that strong non-relativistic winds flow from accretion disks around supermassive black holes and that these winds return most of the mass inflow received from centrally cooling gas. We implement this simple idea by insisting that the outflow velocity remains constant and rather large throughout the biconical jet source region whenever a feedback criterion is satisfied. Although this model for the jet source is admittedly *ad hoc*, as the jets move further out they appear to develop more universal properties. In this section we briefly review the evolution of jets far beyond the source region.

The physical nature of our jets is most clearly defined when the jet activity is continuous in time (models C) such the high resolution model $M11(C, 5, 20, 10)$ in which the overall flow approaches a quasi-steady state. The global velocity field and density contours for the $M11(C, 5, 20, 10)$ flow after 7 Gyrs are shown in Figure 6. The magnitude of the radial gas flow at time 7 Gyrs in three angular directions are shown in Figure 7. It is apparent from this Figure that the cooling inflow, which fills most of the cluster volume, flows toward the jet, becomes entrained and is carried outward. The continuous jet creates an extended two-sided channel of low density gas. The difficulty of observing such a channel can be seen in the X-ray surface brightness images of the (high resolution) $M1(A, 5, 10, 10)$ and $M11(C, 5, 20, 10)$ flows shown in Figure 8, viewed perpendicular to the jet. From this viewing direction the jet cavitation in the continuous $M11(C, 5, 20, 10)$ flow produces at most a 10% reduction in the X-ray surface brightness along the jet axis. The jet cavitation produced by intermittent flows such as $M1(A, 5, 10, 10)$ is less pronounced and more difficult to detect. Although our 2D jets are constrained to flow in a axisymmetric fashion along the $\theta = 0$ and π axes, in a full 3D simulation the jets may not follow such a perfectly linear pathway through the cluster gas.

The symmetric jet cavitations visible in Figure 8 are remarkably similar to the *Chandra* observations of the double-jetted radio galaxy NGC 1265 by Sun, Jerius & Jones (2005). The X-ray contours in their Figure 1a show symmetric indentations along the radio jet axis just as in our Figure 8, suggesting that ambient hot gas in NGC 1265 is being entrained and swept along with the jet. This observation also supports the biconical outflow geometry that we assume here rather than disk winds in the equatorial plane (e.g. Proga 2000).

It is apparent from Figure 8 that our jets are poorly resolved, often occupying only a few angular zones even at the higher grid resolution. This poor resolution restricts somewhat our analysis of the transverse jet profiles. Nevertheless, the behavior of the gas outside of the small jet regions – which determines the overall X-ray properties of the cluster – does not appear to be strongly affected by the level of numerical resolution in the jets.

To understand better the details of the jet-

atmosphere interaction, we have examined the high resolution jet in the $M11(C, 5, 20, 10)$ flow. One natural attribute of the biconical jet source region is that the original gas within the source is expelled very rapidly after the jet turns on. Consequently, during most of the active phase of this region, most of the outgoing gas is supplied by recent advection near the outer boundary of the bicone. As a result, most of the mass outflowing from the jet at r_j occurs near θ_j so the initial jet density profile perpendicular to the jet axis is hollow with a strong central minimum. This type of hollow jet structure may in fact be physically appropriate if entrainment of ambient gas occurs near the source region.

An important feature of these jet solutions is the narrowing of the jets as they moves outward. Although the half angle of biconical jets θ_j can be rather large, these initially conical jets become nearly cylindrical as they move outward. This jet focusing occurs because the pressure in the jet is rapidly lowered by expansion and tends to decrease with radius faster than the pressure in the ambient gas. As a result the jets are compressed and collimated by the ambient gas pressure.

A number of (poorly resolved) internal shocks appear in the jet flow that we do not describe in detail here. The main effect of these shocks, even inside the jet source region, is to raise the temperature and entropy within the central jet to rather high values. Gas in the jet source and just beyond flows approximately at the sound speed within the jet. As the jet moves further out, the mass outflow in the jet increases due to entrainment. The amount of entrainment is approximately independent of the spatial resolution. The top panel in Figure 9 shows the variation of the (outward) mass flux transverse to the jet axis in the continuous $M11(C, 5, 20, 10)$ jet at various cluster radii. The quantity plotted is $d\dot{M}/d\theta = \rho v_r 2\pi r^2 \sin(\theta)\ M_\odot\ \mathrm{yr}^{-1}$ where $v_r(\theta)$ is the local jet velocity. It is clear from Figure 9 the angular width of the jet narrows from its initial half angle $\theta_j = 20^\circ$ as it moves out and remains hollow to rather large distances in the cluster.

Of particular interest is the radial increase of the integrated mass flow in the jet, $\dot{M}(\theta) = \int_0^\theta (d\dot{M}/d\theta) d\theta$, plotted in the lower panel of Figure 9. The total mass outflow in the jet and its approximate local angular width $\theta_{max}(r)$, can be estimated from the maximum $\dot{M} = \dot{M}(\theta_{max})$ in each curve. The decline in $\dot{M}(\theta)$ for $\theta > \theta_{max}$ is due to the negative contribution to the integrated flow beyond θ_{max} caused by slowly inflowing gas adjacent to the jet. The mass flux increases from 65 $M_\odot$/yr at 5 kpc to 116 $M_\odot$/yr at 20 kpc and reaches 170 $M_\odot$/yr at 200 kpc. This increase shows that mass entrainment is a key feature of the success of these simulations. For model $M11(C, 5, 20, 10)$ in which the jet is continuously active, $\dot{M}(\theta = 90^\circ)$ becomes essentially zero, indicating that the jet is returning mass to large radii at the same rate that it arrives at the center in the cooling inflow outside the jet. This mass conservation is approximately true for all the other flows, for example $\dot{M}(90^\circ) \approx -12 \pm 4\ M_\odot$/yr for the flows plotted in Figure 4.

We find that the decelerating jets penetrate to large distances in the cluster gas, well beyond several hundred kpc. However, the maximum distance to which the jet outflow continues is observed to increase with the refinement of the computational grid and this must be explored in future calculations. In fully 3D versions of the $M11(C, 5, 20, 10)$ jet we expect that the lateral motions of jet due to shear instabilities may cause the jet to dissipate its energy at a somewhat smaller radius.

6. CONCLUSIONS

Subrelativistic jet flows that entrain ambient gas may be the essential key for solving the cluster cooling flow problem: Why the hot gas temperature and density profiles resemble cooling flows but show no spectral evidence for cooling below $\sim T_{vir}/3$ at rates expected from the luminosity L_x. Many scenarios have been previously considered in which the gas is heated by a variety of mechanisms including jets. In most previous jet calculations it has been assumed that the jets are primarily sources of energy that reheat the cluster gas with no significant outward mass transport. Overall, these simulations have not been successful in reducing the cooling rate while maintaining the observed temperature and density profiles for many Gyrs. Because of the large number of cooling core clusters observed, cooling must be sharply reduced or arrested for many Gyrs.

The mass-carrying jets considered here are a variant of the circulation flows we have discussed in which buoyant bubbles provide an outward mass transport while most of the X-ray emission comes from a normal cooling interbubble inflow (Mathews, et al. 2003; Mathews, Brighenti & Boute 2004).

Our computational results for mass-carrying jets are robust in that we find satisfactory multi-Gyr solutions for a significant range of parameters describing the initial central jet outflow. The important global features of our flows are also insensitive to computational resolution. The jet outflow is stimulated by cooling or inflowing gas near the central supermassive black hole, but the success of our longterm solutions is not strongly dependent on the specifics of this feedback mechanism. The natural intermittancy of the feedback generates multiple generations of X-ray cavities similar to those observed in the Perseus Cluster and elsewhere. Nevertheless, the physics at the source of outflow is poorly understood and observational support is limited. More detailed models of mass-carrying jets will be necessary before they can be fully accepted.

One possible objection to the jet driven mass circulation described here is that SNIa-enriched gas that enters the source cone (within the central E

galaxy) is transported out only along the jet axis, unlike the observed iron abundance pattern which is spherically symmetric around the central galaxy (de Grandi et al. 2004). Either the radio jet precesses (Gower, et al. 1982) as in the cluster observed by Gitti et al. (2005) or the jet axis direction was altered by black hole mergers at early times when most of the SNIa iron was produced.

Studies of the evolution of hot gas in elliptical galaxies at UC Santa Cruz are supported by NASA grants NAG 5-8409 & ATP02-0122-0079 and NSF grant AST-0098351 for which we are very grateful.

REFERENCES

Allen, S. W. 2000, MNRAS, 315, 269
Basson, J. F. & Alexander, P. 2003, MNRAS, 339, 353
Blandford, R. D. & Begelman, M. C. 1999, MNRAS, 303, L1
Blandford, R. D. & Payne, D. G. 1982, MNRAS, 199, 883
Blandford, R. D. & Znajek, 1977, MNRAS, 179, 433
Brighenti, F. & Mathews, W. G. 2003, ApJ, 587, 580
Brighenti, F. & Mathews, W. G. 2002, ApJ, 573, 542
Bruggen, M. & Kaiser, C. R. 2002, Nature, 418, 301
Buote, D. A. & Tsai, J. C. 1996, ApJ, 458, 27
Cardiel, N., Gorgas, J. & Aragon-Salamanca, A. 1998, MNRAS, 298, 977
Cavaliere, A., Lapi, A. & Menci, N. 2002 ApJ, 581, L1
Churazov, E., et al. 2005, MNRAS 363, L91
Churazov, E., Sunyaev, R., Forman, W., & Bohringer, H. 2002, MNRAS, 332, 729
Cowie, L. L., Hu, E. M., Jenkins, E. B. & York, D. G. 1983, ApJ, 272, 29
Crenshaw, D. M., et al. 1999, ApJ, 516, 750
Dalla Vecchia, C. et al. 2004, MNRAS, 355, 955
de Grandi, S., Ettori, S., Longhetti, M., Molendi, S., 2004, A&A, 419, 7
Edge, A. C. 2001, MNRAS, 328, 762
Ettori, S., Fabian, A. C., Allen, S. W. & Johnstone, R. M. 2002, MNRAS, 331, 635
Fabian, A. C. et al. 2003, MNRAS 344, L43
Fabian, A. C., Sanders, J. S., Ettori, S., Taylor, G. B., Allen, S. W., Crawford, C. S., Iwasawa, K. & Jonstone, R. M. 2001, MNRAS, 321, L33
George, I. M., et al. 1998, ApJS, 114, 73
Gitti, M., Feretti., L., & Schindler, S. 2005, A&A, (in press) (astro-ph/0510613)
Hopkins, P. F., Narayan, R. & Hernquist, L. 2005, ApJ (submitted) (astro-ph/0510369)
Johnstone, R. M., Fabian, A. C. & Nulsen, P. E. J. 1987, MNRAS, 227, 75
Konigl, A. & Kartje, J. F. 1994, ApJ, 434, 446
Everett, J. E., Königl, A. & Kartje, J. F. 2001, ASP Conf. Ser. v. 224, eds. B. M. Peterson, R. S. Polidan & R. W. Pogge, 441
Kriss, G. A., 2004, IAU Symp. 222, (in press) (astro-ph/0403685)
Kriss, G. 2003, A&A, 403, 473
McCarthy, I. G., Babul, A., Katz, N., & Balogh, M. L. 2003, ApJ, 587, 75
Mathews, W. G., Brighenti, F., Buote, D. A. 2004, ApJ, 615, 662
Mathews, W. G., Brighenti, F., Buote, D. A., Lewis, 2003, ApJ 596, 159
Mathews, W. G. & Brighenti, F. 2003, Ann. Rev. Astron. & Ap. 41, 191
McNamara, B. R. 1997, in "Galaxies and Cluster Cooling Flows", ed. N. Soker, ASP Conf. Ser., vol 115, p 109
Narayan, R. & Yi, I. 1994, ApJ, 428, L13
Navarro, J. F., Frenk, C. S., & White, S. D. M. 1996, ApJ, 462, 563
McNamara, B. R. 2001, XXI Moriond conf: "Galaxy Clusters and the High Redshift Universe Observed in X-rays", eds. D. Neumann, F. Durret, & J. Tran Thanh Van
Morganti, R., Tadhunter, C. N. & Oosterloo, T. A. 2005, A&A (submitted) (astro-ph/050263)
Morganti, R., Tadhunter, C. N., & Oosterloo, T. A. 2004, Proc. of teh "Extra-planar Gas" Conference, ASP Conf. Ser. ed R. Baun (in press)
Mittaz, J. P. D. et al. 2001, A&A, 365, L93
Nath, B. B. & Roychowdhury, S. 2002 MNRAS, 333, 145
Omma, H., et al. 2004, MNRAS, 348, 1105
Peterson, J. R. & Fabian, A. C. 2005, Physics Reports (in press)
Pizzolato, F. et al. 2003, ApJ 592, 62
Proga, D. 2003, ApJ, 585, 406
Proga, D. 2000, ApJ, 538, 684
Reynolds, C. S., Heinz, S., & Begelman, M. C. 2002, MNRAS, 332,271
Reynolds, C. S., Heinz, S., & Begelman, M. C. 2001, ApJ, 549, L179
Risaliti, G., Bianchi, S., Matt, G., Baldi, A., Elvis, M., Fabbiano, G., & Zezas, A. 2005, ApJ, 630, L129
Salome, P. & Combes, F. 2004, A$A, 415, L1
Soker, N. & Pizzolato, F., 2005, ApJ, 622, 847
Sun, M., Jerius, D. & Jones, C. 2005, ApJ, 633, 165
Tamura, M. et al. 2001, A&A, 365, L87
Zanni, C. et al. 2005, A&A, 429, 399

TABLE 1
GASDYNAMICAL MODELS

model	feed-back	r_j (kpc)	θ_j (°)	u_j (10^3 km s^{-1})	E_{kin} (10^{62} erg)	L_{mech} (10^{45} erg s^{-1})	L_x (10^{45} erg s^{-1})	M_{cool} (10^{11} $M_\odot$)	$\langle \dot{M} \rangle$ ($M_\odot$ yr^{-1})	comment[a]
(1)	(2)	(3)	(4)	(5)	(6)	(7)	(8)	(9)	(10)	(11)
m1(A,5,10,10)	A	5	10	10	4.90	2.59	2.19	1.20	20.0	OK
m2(A,5,20,10)	A	5	20	10	2.43	1.28	2.63	0.99	16.56	OK
m3(A,5,20,5)	A	5	20	5	1.45	0.77	3.23	3.72	62.1	marginal
m4(B,5,10,10)	B	5	10	10	6.71	3.54	2.19	1.50	25.1	OK
m5(B,5,10,5)	B	5	10	5	1.16	0.61	2.87	9.14	152.4	fails
m6(B,5,20,10)	B	5	20	10	5.54	2.93	2.17	0.016	0.27	OK
m7(B,5,20,5)	B	5	20	5	2.10	1.11	2.65	0.47	7.88	OK
m8(B,5,20,1)	B	5	20	1	0.11	0.054	2.31	21.5	359	fails
m9(A,3,20,10)	A	3	20	10	2.80	1.48	2.62	3.81	63.5	marginal
m10(A,3,20,5)	A	3	20	5	1.67	0.88	2.83	6.22	104	fails
m11(C,5,20,10)	C	5	20	10	0.087	0.046	2.18	0.016	0.27	OK
m12(C,5,20,5)	C	5	20	5	0.40	0.21	2.65	0.47	7.88	OK
m13(B,5,10,10)[b]	B	5	10	10	7.65	4.09	2.11	~ 0.02	~ 0	OK
m14(B,5,10,5)[b]	B	5	10	5	7.36	3.88	1.94	~ 0	~ 0	OK

[a]Evaluation of the relative success of each computed flow after $t = 7$ Gyrs is based primarily on requiring $\langle \dot{M} \rangle \lesssim 50\ M_\odot\ \mathrm{yr}^{-1}$.
[b]In these models $q(T) = 0$.

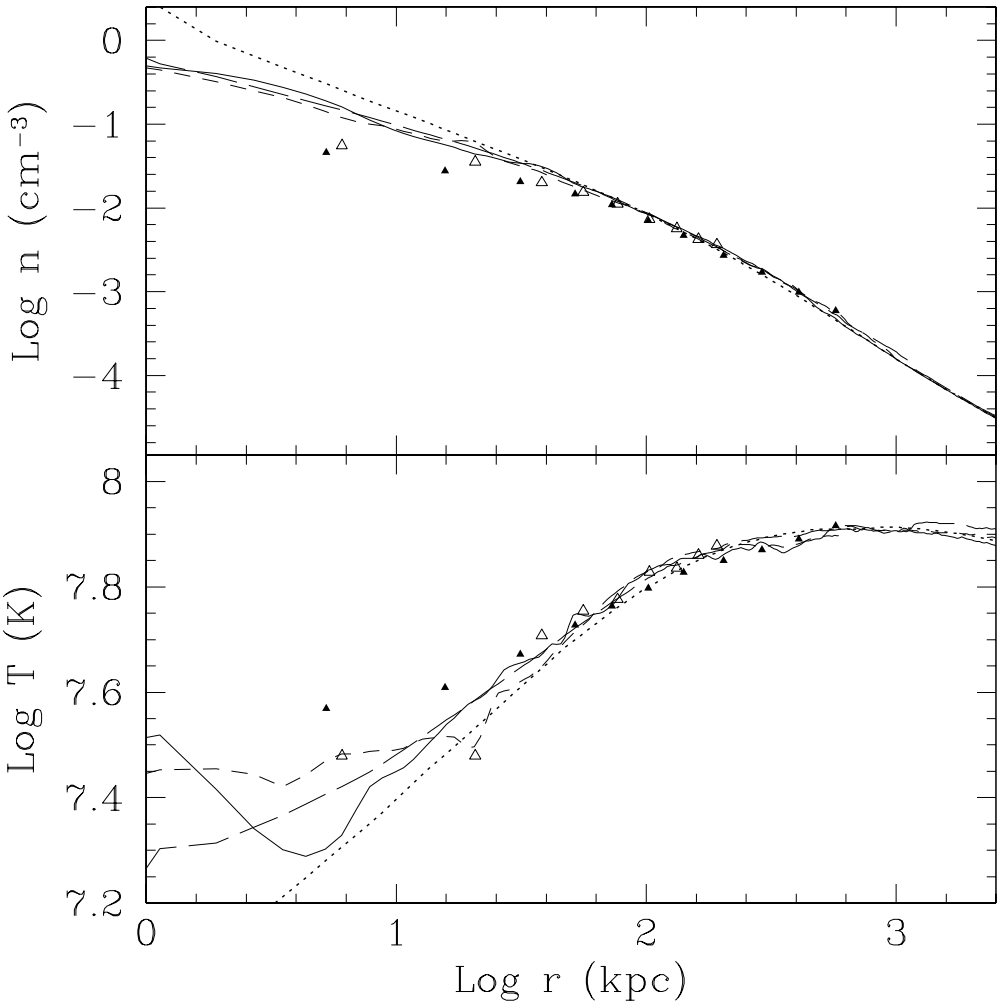

FIG. 1.— The observed hot gas density and temperature in A1795 are shown with filled triangles (*XMM* observations from Tamura et al. 2001) and open triangles (*Chandra* observations from Ettori et al. 2002). The dotted line shows the quasi-steady pure cooling flow at time $t = 7$ Gyrs. The other lines show the computed density and temperature profiles for flow $m1(A, 5, 10, 10)$ at three times: 2 Gyrs (*long-dashed lines*), 4 Gyrs (*short-dashed lines*),and 6 Gyrs (*solid lines*).

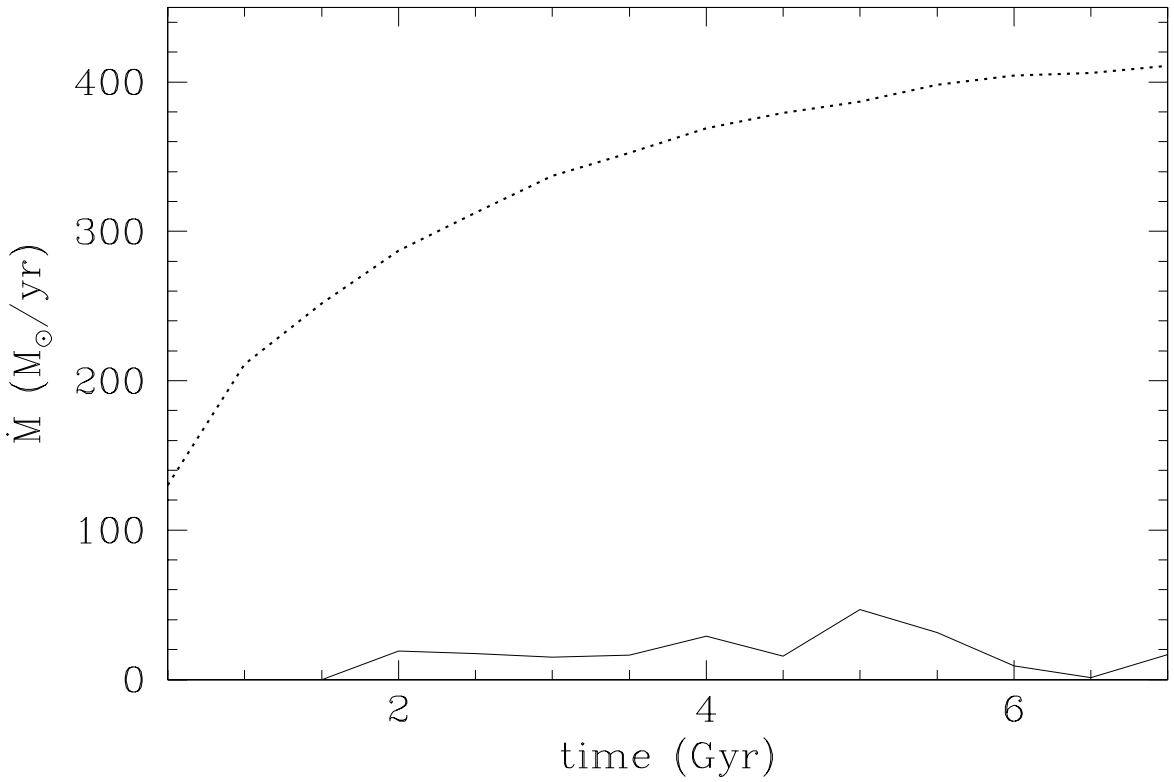

FIG. 2.— The total cooling rate $\dot{M}(t)$ for the cooling flow solution (*dotted line*) and for flow $m1(A, 5, 10, 10)$ (*solid line*).

FIG. 3.— The density distribution for flow calculation $M1(A, 5, 10, 10)$ at four times.

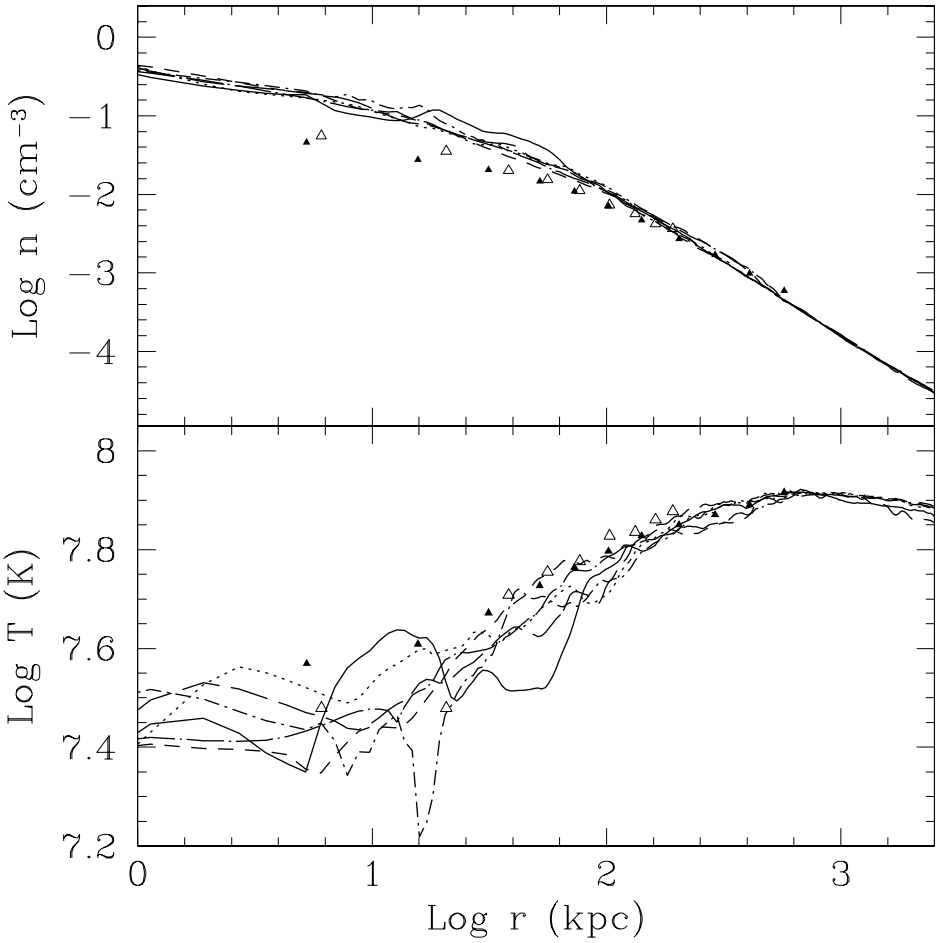

FIG. 4.— Density and temperature profiles at time $t = 7$ Gyr for six computed flows: m3(A,5,20,5) (*solid line*), m9(A,3,20,10) (*long-dashed line*), m7(B,5,20,5) (*short-dashed line*), m10(A,3,20,5) (*short dashed-dotted line*), m12(C,5,20,5) (*long dashed-dotted line*), and m7(B,5,20,5) (*dotted line*).

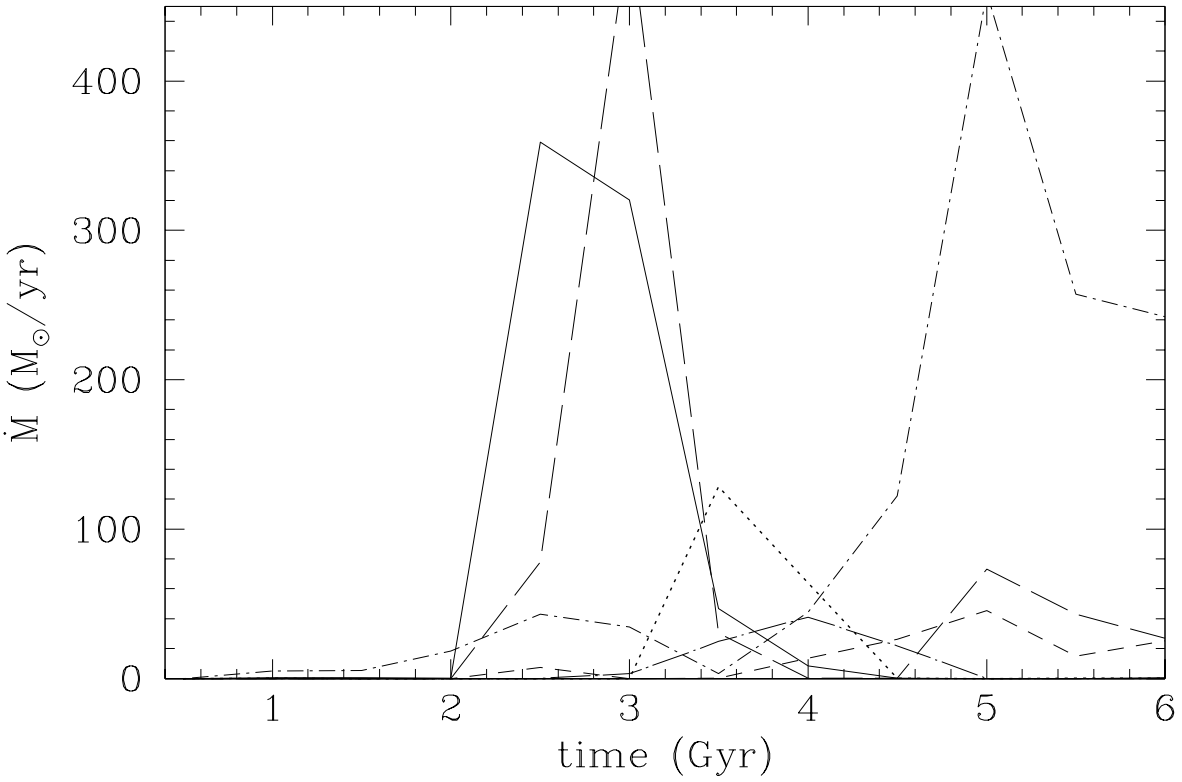

FIG. 5.— Total cooling rates $\dot{M}(t)$ for six computed flows: m3(A,5,20,5) (*solid line*), m9(A,3,20,10) (*long-dashed line*), m7(B,5,20,5) (*short-dashed line*), m10(A,3,20,5) (*short dashed-dotted line*), m12(C,5,20,5) (*long dashed-dotted line*), and m7(B,5,20,5) (*dotted line*).

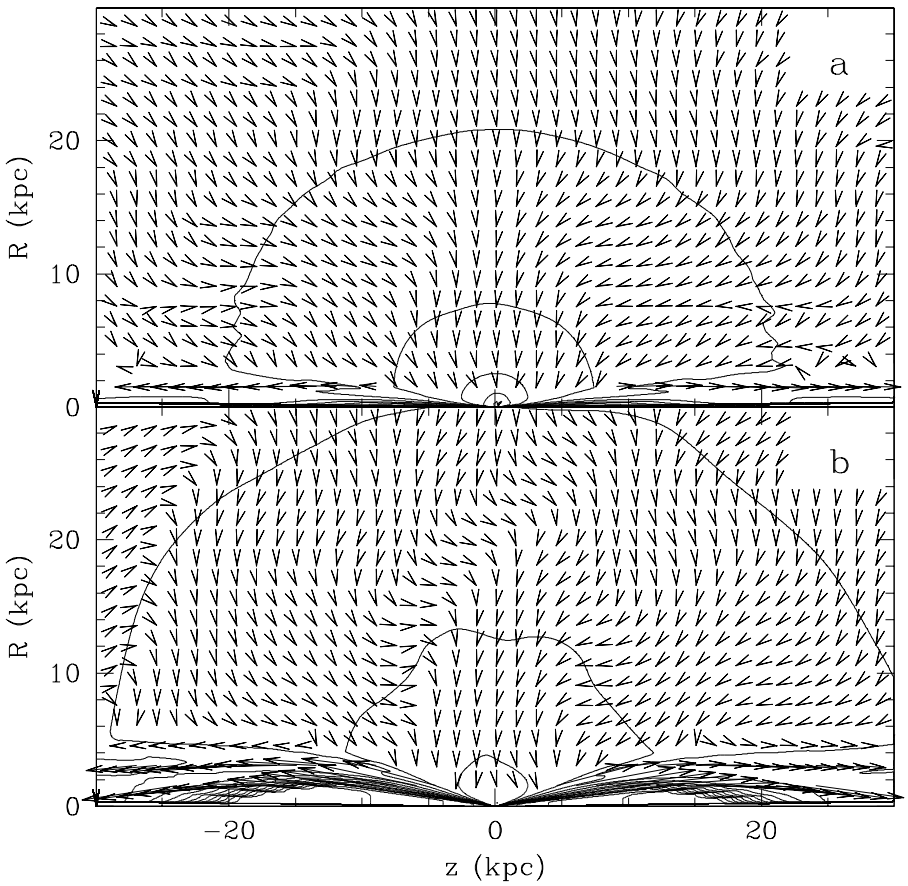

FIG. 6.— Velocity flow superimposed on gas density contours for the central region of computed flow $M11(C, 5, 20, 10)$ shown in cylindrical coordinates. The jet becomes narrower as it moves out.

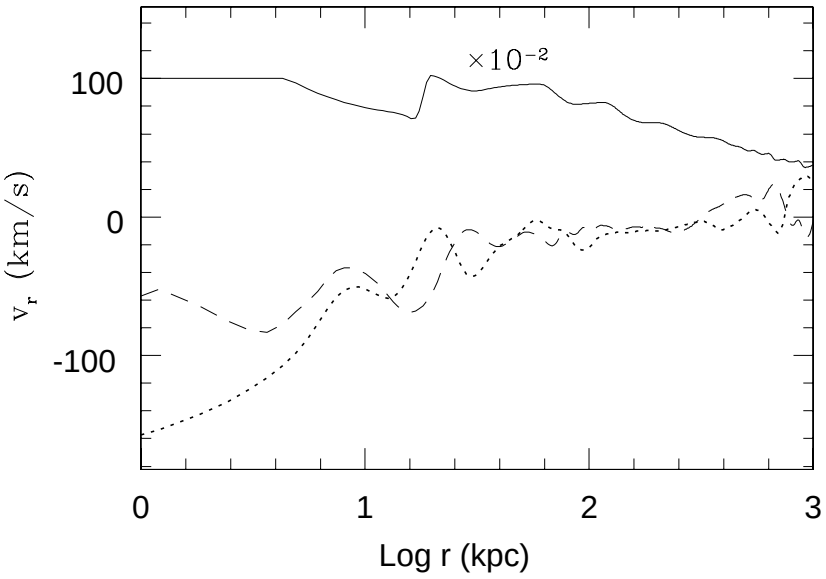

FIG. 7.— A snapshot of the radial gas velocity profiles in model $M11(C, 5, 20, 10)$ at time $t = 7$ Gyrs along three angular directions: the axial jet outflow at $\theta = 0$ (*solid line*), in which the plotted velocities have been reduced by 10^{-2}, $\theta = \pi/4$ (*dashed line*), and the equatorial flow at $\theta = \pi/2$ (*dotted line*).

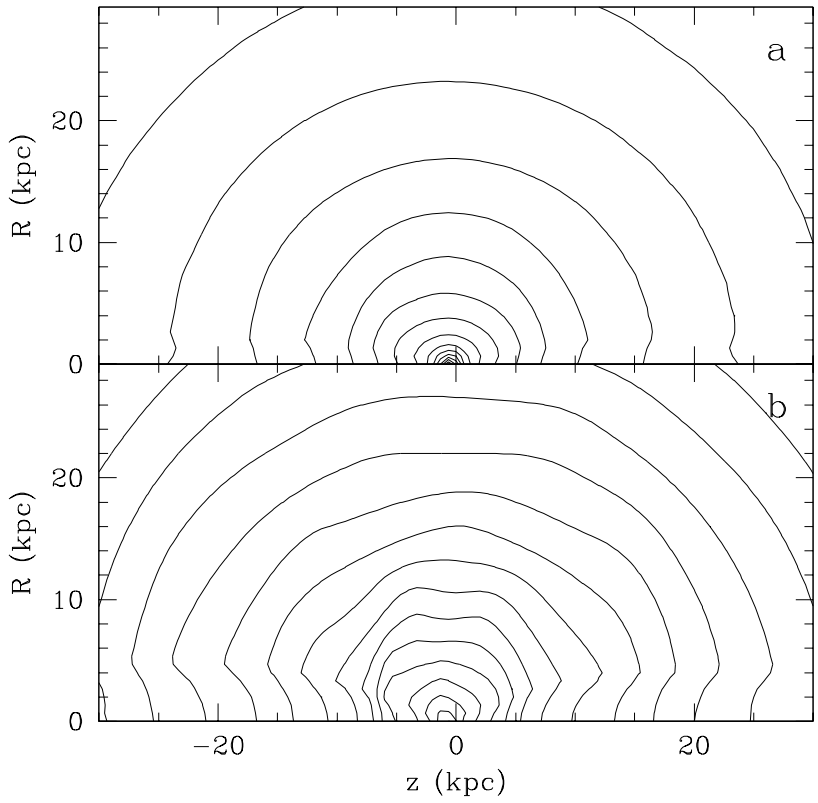

FIG. 8.— Contours of the bolometric X-ray surface brightness for flows M1(A,5,10,10) (top panel) and M11(C,5,20,10) (bottom panel) at time $t = 7$ Gyrs.

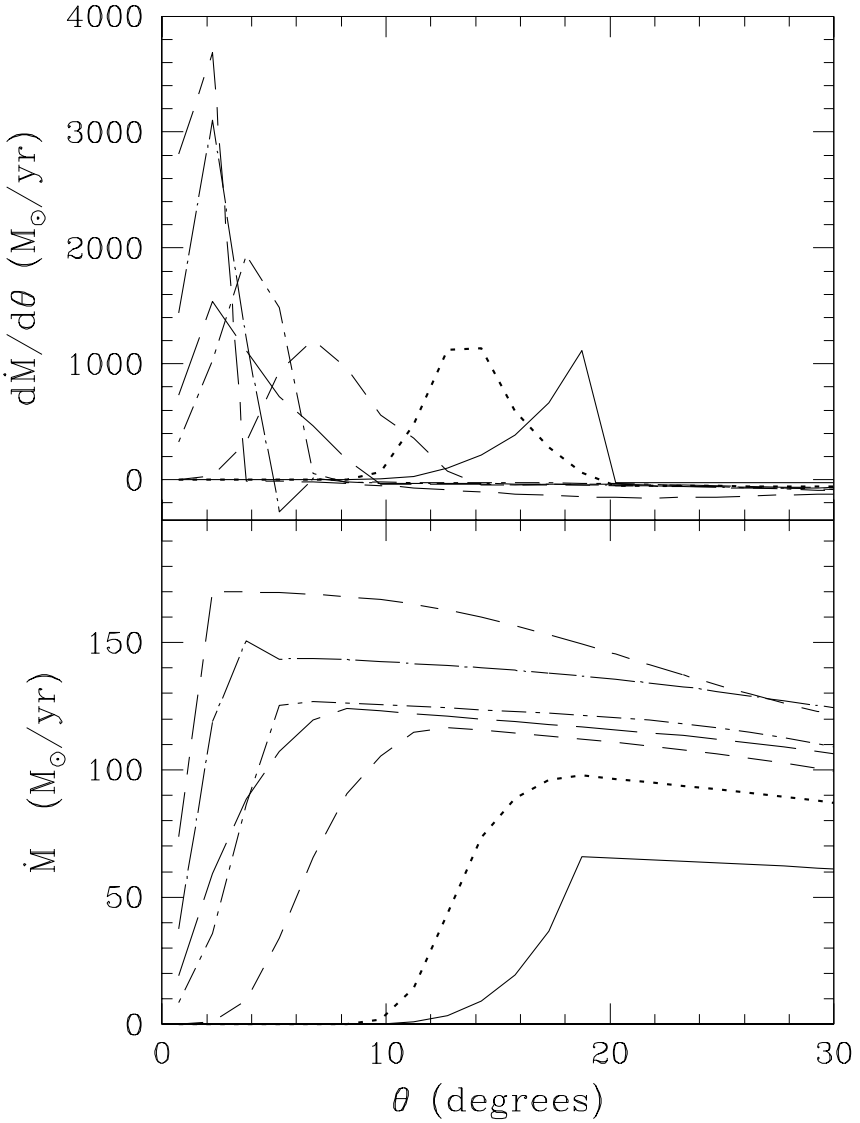

FIG. 9.— Angular variation of the jet flow $d\dot{M}/d\theta$ (top panel) and the integrated jet flow $\dot{M}(\theta)$ to (half) angle θ (bottom panel) computed for the continuous jet model M11(C,5,20,10). Both profiles are shown for seven cluster radii: 5 kpc (*solid line*) 10 kpc (*dotted line*) 20 kpc (*short dashed line*) 30 kpc (*long dashed line*) 50 kpc (*short dashed-dotted line*) 100 kpc (*long dashed-dotted line*) and 200 kpc (*short and long dashed line*).

This figure "f3color.jpg" is available in "jpg" format from:

http://arXiv.org/ps/astro-ph/0601555